Smart Structures and Systems, *Vol. 30, No. 3 (2022) 245-253*
https://doi.org/10.12989/sss.2022.30.3.245

Microstructural modeling of two-way bent shape change of composite two-layer beam comprising a shape memory alloy and elastoplastic layers

Fedor S. Belyaev [1], Margarita E. Evard [2], Aleksandr E. Volkov*[2], Natalia A. Volkova [3] and Egor A. Vukolov [2]

[1] *Institute for Problems in Mechanical Engineering of the Russian Academy of Sciences, Boljshoy prospekt V.O. 61, 199178,Saint-Petersburg, Russia*
[2] *Saint-Petersburg State University, 7-9 Universitetskaya Embankment, 199034 St Petersburg, Russia*
[3] *St. Petersburg State Technological Institute (Technical University), 26 Moskovski ave., 190013 St. Petersburg, Russia*

(*Received May 18, 2022, Revised July 16, 2022, Accepted July 16, 2022*)

Abstract. A two-layer beam consisting of an elastoplastic layer and a functional layer made of shape memory alloy (SMA) TiNi is considered. Constitutive relations for SMA are set by a microstructural model capable to calculate strain increment produced by arbitrary increments of stress and temperature. This model exploits the approximation of small strains. The equations to calculate the variations of the strain and the internal variables are based on the experimentally registered temperature kinetics of the martensitic transformations with an account of the crystallographic features of the transformation and the laws of equilibrium thermodynamics. Stress and phase distributions over the beam height are calculated by steps, by solving on each step the boundary-value problem for given increments of the bending moment (or curvature) and the tensile force (or relative elongation). Simplifying Bernoulli's hypotheses are applied. The temperature is considered homogeneous. The first stage of the numerical experiment is modeling of preliminary deformation of the beam by bending or stretching at a temperature corresponding to the martensitic state of the SMA layer. The second stage simulates heating and subsequent cooling across the temperature interval of the martensitic transformation. The curvature variation depends both on the total thickness of the beam and on the ratio of the layer's thicknesses.

Keywords: bending; boundary-value problem; modelling; shape memory alloys

1. Introduction

Many applications of shape memory alloy (SMA) require generation of large displacements. Among them are actuators (see Duerig *et al*. 1990, Wanhill and Ashok 2017, Jani *et al*. 2014), passive vibration control re-centering devices (Torra *et al*. 2014, Casciati 2019), medical staples (Zhang *et al*. 2013), endovascular stents (Petrini *et al*. 2017), etc. One of the ways to obtain large displacements is to use SMA parts functioning in bending mode. In some applications a repeated action is needed. It can be based on the effect of two-way shape memory or on the use of a bias part creating an opposing force and thus storing elastic energy on the stage of heating and securing repeated straining on consequent cooling. The latter way proved to be reliable in many applications (Jani *et al*. 2014). If the active member of an actuator operates in bending mode the functional part and the bias part can be combined in one composite beam, one layer of which is made of SMA and the other of an elastoplastic material. This engineering solution can lead to simplicity and compactness of the actuator. An efficient method to produce such two-layer beam is the method of explosion welding (Prummer and Stockel 2001). In the works by Belyaev *et al*. (2011) it was shown that pressure developed under explosion does not hinder the martensitic transformation and there is no embrittlement in the weld.

Bending is characterized by inhomogeneous stress with tension on one side of the beam and compression on the opposite side. To find the evolution of the stress field and curvature of the beam under the action of the bending moment and temperature it is necessary to solve the boundary value problem. The constitutive relations must be capable to describe the peculiarities of SMA mechanical properties such as phase – temperature and stress – strain hysteresis, tension – compression asymmetry inherent to TiNi-based SMA (Volkov *et al*. 2013, Chatziathanasiou *et al*. 2015).

At present success was achieved in solving isothermal problems for SMA in the pseudoelastic or pseudoplastic state. A macroscopic model (Auricchio and Petrini 2002) is implemented into a finite element program ANSYS (Ansys® Academic Research Mechanical APDL, Release 14.0). Simoes and Martínez-Pañeda (2021) using a macro model based on the approach of D.C. Lagoudas (Lagoudas 2008) solved a 2D problem calculating the stress near a crack tip. They introduced a fatigue degradation function and found the cyclic life of a medical stent. For non-isothermal loading only the simplest 1D problems, such as torsion of a cylinder with the fixed inner surface and a

*Corresponding author, Professor,
E-mail: a.volkov@spbu.ru

ISSN: 1738-1584 (Print), 1738-1991 (Online)

turned outer surface (Rogovoy and Stolbova 2019), expanding and assembling of a thermomechanical coupling (Likhachev *et al*. 1997), tension of a cylinder loaded with axial force and cooled from the surface (Volkov and Kukhareva 2008, Volkov *et al*. 2017, Kukhareva *et al*. 2020). In these works, a microstructural model was used. It allowed obtaining description of SMA behavior under simultaneous variation of stress and temperature but demanding rather much computation time. In the work (Volkov *et al*. 2019) a problem of pure bending of a TiNi beam in the isothermal conditions in the austenitic pseudoelastic and martensitic pseudoplastic state was considered. The present article extends these results to simulation of preliminary straining of a two-layer SMA-elastoplastic beam and the curvature variation on consequent heating, and cooling.

2. Microstructural model

The basic ideas of microstructural modeling are: (1) account for the structure of the SMA by considering two or more structural levels with calculation of the macroscopic strain by averaging of the micro-strains; (2) formulation of the constitutive relations for micro-strains basing on the physical regularities governing different deformation processes. These principles allow physically grounded description of the functional-mechanical behavior of metallic alloys, including SMA. For SMA some of the first such models were reported in the works (Erglis *et al*. 1995, Patoor *et al*. 1996, Huang and Brinson 1998). In the works by Patoor *et al*. (1996), and Huang and Brinson (1998) the primary martensite orientation variants are considered to be plates characterized by the invariant plane and the direction of shear. J. Eshelby's theory is applied to calculate the interaction energy between the plates. These variants can form self-accommodated groups in which they can grow cooperatively. It is shown that these models can simulate pseudoelasticity and the shape memory effect. Further development of E. Patoor, A. Eberhardt, and M. Berveiller model (Patoor *et al*. 1996) was made in Niclaeys *et al*. (2004), in which the interaction matrix for martensite variants in NiTi SMA was derived. This matrix accounted for all self-accommodating groups observed in this alloy.

Works (Fischlschweiger *et al*. 2011, Oberaigner and Leindl 2012) were probably the first, in which there was suggested an idea of connecting the thermodynamic principles with the apparatus of statistical physics. In the work by Fall *et al*. (2019) the Boltzmann-type statistical approach was applied to crystal plasticity. In both cases, a self-consistent scheme of the transition from the stresses and strains in micro volumes to the macro scale was used.

The microstructural approach, used in this work, was described in (Erglis *et al*. 1995, Evard and Volkov 1999, Volkov and Casciati 2001) and extended to account for the micro-plastic deformation and fracture in the work by Evard *et al*. (2006, 2015) and for the account of plastic deformation in the work Belyaev *et al*. (2022). The primary orientation variants of martensite are the domains, which originate from austenite by one of the Bain's variants of the

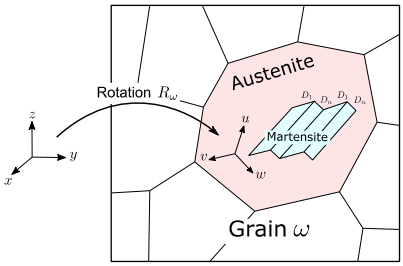

Fig. 1 Scheme of the representative volume of SMA

lattice transformation. This model allows simulating all the basic functional-mechanical properties of SMA. The representative volume V of SMA (Fig. 1) consists of a set of grains, each characterized by the orientation ω of its crystallographic axes. Inside each grain there are martensite variants and austenite.

A. Reuss' hypothesis is adopted: the macroscopic strain ε (small strain tensor) is calculated by neutralization of all micro strains. Spatial averaging of the micro-strains is substituted by averaging over grains orientations. Thus, the macroscopic strain tensor ε and the volume fraction Φ_M of martensite are

$$\varepsilon = \frac{1}{N_{gr}} \sum_{\omega=1}^{N_{gr}} \varepsilon^{gr}(\omega), \quad \Phi_M = \frac{1}{N_{gr}} \sum_{\omega=1}^{N_{gr}} \Phi^{gr}(\omega)$$

where the sum is taken over all grains, N_{gr} is the number of grains, $\varepsilon^{gr}(\omega)$, $\Phi^{gr}(\omega)$ are the strain and the volume fraction of martensite in grain ω.

The strain of each grain is assumed to be the sum of the elastic ε^e, thermal ε^T, phase ε^{Ph} and micro-plastic ε^{MP} strains

$$\varepsilon^{gr} = \varepsilon^e + \varepsilon^T + \varepsilon^{Ph} + \varepsilon^{MP}$$

(argument ω in this and the next formulae is omitted). The martensite volume fraction in a grain Φ^{gr}, the phase strain ε^{Ph} due to the crystal lattice deformation during martensitic transformation and the micro-plastic strain ε^{MP} occurring near the martensite phase crystals are calculated by the formulae

$$\Phi^{gr} = \frac{1}{N} \sum_{n=1}^{N} \Phi_n, \quad \varepsilon^{Ph} = \frac{1}{N} \sum_{n=1}^{N} \Phi_n D_n,$$

$$\varepsilon^{MP} = \frac{1}{N} \sum_{n=1}^{N} \kappa_{MP} \varepsilon_n^P dev D_n,$$

where the sum is taken over all martensite variants, N is the number of variants, $(1/N)\Phi_n$ is the volume fraction of the n-th martensite variant in the grain, D_n is the n-th variant lattice deformation tensor and devD_n is its deviator, ε_n^P are internal variables serving as the measures of the micro-plastic strain, κ_{MP} is a material constant. The third formula is written by an analogy with the second and expresses the idea that the micro-plastic deformation caused by the growth of martensite can be expanded in the sum similar to that for the phase strain. The elastic and thermal strains are supposed isotropic and calculated as the weighted sum

(with the weights 1–Φ^{gr} and Φ^{gr}) of the strains of austenite and martensite using the common Hook's law and the law of thermal expansion.

The evolution equations for the variables Φ_n and $\varepsilon_n^{\mathrm{P}}$ are formulated in terms of the generalized thermodynamic forces, which are the derivatives of the Gibbs' potential G, which for a unit volume can be written as

$$G = G^{eig} + G^{mix} = (1 - \Phi^{gr})G^{A} + \frac{1}{N}\sum_{n=1}^{N} \Phi_n G^{Mn} + G^{mix}$$

where G^{A} and $G^{\mathrm{M}n}$ are the eigen potentials of austenite and martensite (without an account of their interaction) and G^{mix} is the "mixing" potential equal to the elastic energy of the interphase stresses. This energy is estimated by the formula

$$G^{mix} = \frac{\mu}{2}\sum_{m,n=1}^{N} A_{mn}(\Phi_m - b_m)(\Phi_n - b_n)$$

where A_{mn} are the coefficients, accounting for the interaction between the variants, μ is a material constant and b_n are the internal variables accounting for the relaxation of the elastic energy of the interphase stresses caused by the micro-plastic deformation. These variables can be interpreted as the densities of the oriented deformation defects (dislocation loops generated in the course of the plastic accommodation. In the work by Nae *et al*. (2003), potential G^{mix} is referred to as the "phase interaction energy function" (PIEF). The eigen potentials G^{A} and $G^{\mathrm{M}n}$ are expressed by the formula

$$G^{a} = G_0^{a} - S_0^{a}\cdot(T - T_0) - \frac{c_\sigma^{0a}(T - T_0)^2}{2T_0} - \varepsilon_{ij}^{0Ta}(T)\sigma_{ij} - \frac{1}{2}D_{ijkl}^{a}\sigma_{ij}\sigma_{kl}, \qquad a = A, Mn$$

where superscript a stands for A (Austenite) and Mn (n-th variant of Martensite); T is the temperature; T_0 is the temperature of the thermodynamic equilibrium of austenite and martensite at zero stress; σ_{ij} are the Cauchy stress components; $G_0{}^a$, $S_0{}^a$ are the values of the Gibbs' potential and of the entropy at $T = T_0$ and $\sigma = \sigma_0 = 0$; $\varepsilon^{0Ta}(T)$ is the strain at temperature T and $\sigma = \sigma_0$; $c_\sigma{}^{0a}$ is the specific heat (per unit volume); $D^a{}_{ijkl}$ are components of the tensor of elastic compliances. For temperature T_0 the estimate $T_0 = (M_{\mathrm{s}} + A_{\mathrm{f}})/2$ suggested and substantiated in work (Salzbrenner and Cohen 1979) is used, where M_{s} and A_{f} are the temperatures of the start of the forward and of the finish of the reverse transformations.

For TiNi SMA the forward transformation is from the cubic phase into monoclinic with the number of orientation variants of martensite $N = 12$. An account of shuffles would increase this number up to 24, but the shuffles do not affect the homogeneous part of the phase strain. The Bain's variants in TiNi are grouped into the "Corresponding Variants Pairs" (CVP) (Nishida *et al*. 2012a, b, Imamura *et al*. 2012). In the present model this feature is accounted for by the matrix (A_{mn}), which for a proper numeration of variants is proposed as

$$\mathrm{A} = \begin{pmatrix} A_1 & 0 & 0 \\ 0 & A_1 & 0 \\ 0 & 0 & A_1 \end{pmatrix}, \quad A_1 = \begin{pmatrix} 1 & -\alpha & -\alpha & 0 \\ -\alpha & 1 & 0 & -\alpha \\ -\alpha & 0 & 1 & -\alpha \\ 0 & -\alpha & -\alpha & 1 \end{pmatrix}, \quad (1)$$

where α is a material constant ($0 \le \alpha < 1/2$) measuring the degree of the interaction between the variants forming a CVP. The evolution equation for the internal variables is deduced from the transformation condition

$$F_n = \pm F^{\mathrm{fr}},$$

where

$$F_n = -\frac{\partial G}{\partial \Phi_n} \approx \frac{q_0(T - T_0)}{T_0} + \sigma_{ij}: \quad (D_n)_{ij} - \mu\sum_{m=1}^{N} A_{nm}\,\Phi_m$$

is the driving thermodynamic force of the transformation and F^{fr} is the dissipative ("friction") force. Sign "+" stands for the direct and "–" for the reverse transformation; q_0 is the latent heat of the transformation ($q_0 < 0$). From the transformation condition it follows that the transformation occurs at a state apart from equilibrium (when there is an excess of the driving force).

For the reorientation (twinning) of martensite three hypotheses are accepted: (1) any variant of martensite can be transformed in any other variant; (2) reorientation occurs along the direction in the space $\Phi_1,\ldots, \Phi_N$, corresponding to the fastest decrease of the Gibbs' potential; (3) reorientation starts when the thermodynamic force reaches a critical value. From these hypotheses it follows that reorientation will occur along the projection L of the vector

$$F = \{F_n\} = \{-\partial G/\partial\Phi_1, \ldots, -\partial G/\partial\Phi_n\}$$

on the plane $\Phi_1 + \ldots + \Phi_N$ = const. If for some n it holds that $\Phi_n = 0$ and $L_n < 0$, L must be substituted for its projection L' onto the intersection of planes $\Phi_n = 0$ and $\Phi_1 + \ldots + \Phi_N$ = const. Then the condition of reorientation is postulated as

$$-\partial G/\partial L = F^{fr\,tw}$$

where $F^{\mathrm{fr\,tw}}$ is a material constant, characterizing the critical driving force for reorientation.

To find the evolution of internal variables ε_n^{P} and b_n the micro-plastic flow condition is formulated

$$|F_n^P - F_n^{\varrho}| = F_n^{y}$$

where $F_n^P = -\partial G/\partial b_n$ is the driving force of the micro-plastic flow caused by the growth of the n-th variant of martensite, F_n^{ϱ} and F_n^{y} are forces characterizing the kinematic and isotropic hardening. Note that the micro-plastic flow condition is analogous to the 1D classic plastic flow condition

$$|\sigma - \varrho| = \sigma_y$$

with F_n^P playing the role of the stress σ, F_n^{ϱ}– of the back stress ϱ and F_n^{y}–of the flow stress σ_y. The micro-plastic flow produces deformation defects. In this model two types of the defects are distinguished: oriented defects b_n creating long-range stress fields and scattered defects f_n, which are

obstacles to plastic flow. In the proposed model forces F_n^{ϱ} and F_n^{y} are related to oriented defects b_n and scattered defects f_n by the simplest formulae

$$F_n^{\varrho} = a_{\varrho} b_n, \qquad F_n^{y} = a_y f_n,$$

where a_{ϱ} and a_y are material constants.

To describe the variation of the defect densities the evolution equations were formulated

$$\dot{b}_n = k_b \dot{\varepsilon}_n^P - \left(\frac{|b_n|}{\beta^*}\right) \dot{\varepsilon}_n^P H(b_n \dot{\varepsilon}_n^P) + r_b(T) \left(\frac{|F_n^P|}{\mu}\right) sign(F_n^P),$$

$$\dot{f}_n = |\dot{\varepsilon}_n^P| - r_f(T)(f_n - f_0),$$

where H denotes Heaviside's step function, k_b, β^* and f_0 are material constants, $r_b(T)$ and $r_f(T)$ are Arrhenius type functions of temperature. The first term in the right-hand part of the equation for $\dot{b}_n$ describes the oriented defects production in the course of the micro-plastic flow, the second term accounts for the escape of the defects to the outer surface and the third – evolution of the defects in time while the driving force F_n^P of the micro-plastic flow is non-zero. In the equation for $\dot{f}_n$ the first term in the right-hand part of the equation describes production of the scattered defects in the course of the micro-plastic flow and the second – their decrease due to relaxation processes.

The values of the material constants for TiNi SMA were determined in a previous work (Evard *et al*. 2015).

This microstructural approach proved to be efficient for simulating the deformation of a specimen in different states (martensitic, two-phase, and austenitic) as well as strain accumulation on cooling and heating under a constant or varying load.

3. Boundary-value problem for bending of an SMA beam

A finite element model is developed to represent a cracked beam element of length d and the crack is located at Consider a two-layer beam with width b and total thickness h, loaded by a bending moment M or/and an axial force F as shown in Fig. 2. We assume isothermal conditions, i.e., the case when the heat transfer occurs fast and the temperature can be considered homogeneous. The beam consists of two layers: the "upper" layer with thickness h_1 made of SMA and the "lower" layer with thickness h_2 made of an elastoplastic material (steel). We make a simplifying assumption that the Bernoulli plane-sections hypothesis and the hypothesis of non-compression of layers can be applied. In this case, the strain distribution over the thickness of the beam is specified by the formula

$$\varepsilon_{zz}(y) = \kappa y + \bar{\varepsilon},$$

where κ is the curvature of the beam central layer and $\bar{\varepsilon}$ is the relative elongation of this layer. The only non-vanishing stress is σ_{zz}. Further, notations ε and σ are used for ε_{zz} and σ_{zz}.

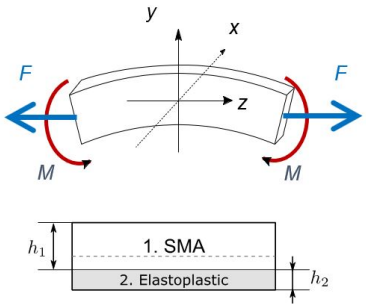

Fig. 2 Scheme of loading

According to Hook's law

$$\sigma = E(\varepsilon - \varepsilon^{ne}),$$

where E is Young's modulus and ε^{ne} is the non-elastic strain.

The equilibrium conditions for the force and the moment are

$$\int_{-h/2}^{h/2} b\sigma(y)dy = F, \qquad \int_{-h/2}^{h/2} b\sigma(y)ydy = M$$

Note that similar approach to the problem of SMA beam bending was used by Li *et al*. (2006); and Yang and Seelecke (2008). The increments of the phase strain and of the internal variables for given increments of the stress and the temperature are given by the microstructural model described in Section 2. This model sets the two functions F_1 and F_2, such that

$$\Delta\varepsilon^{ne}(y) = F_1\big(\Delta T, \Delta\sigma(y), X(y)\big),$$
$$\Delta X(y) = F_2\big(\Delta T, \Delta\sigma(y), X(y)\big),$$

where X denotes the set of the internal variables of the model. For the elastoplastic layer a common bi-linear stress-strain diagram is used.

To solve the problem we discretize the interval [–h/2 , h/2] into K equal segments and search for the values σ_j, = $\sigma(y_j)$, ε_j, = $\varepsilon(y_j)$, where $y_j = (jh/K)$, $j = 0,\ldots, K$).

We split the whole problem into two parts. The first problem is the problem of the mechanical equilibrium and it is finding the "vector" $\{\sigma_j\}$ for given moment M, force F and "vector" of non-elastic strain $\{\varepsilon_j^{ne}\}$. Denoting the operator solving this problem by M, we have

$$\{\sigma_j\} = M\big(M, F, \{\varepsilon_j^{ne}\}\big).$$

The second ("rheological") problem is to find the increments of the non-elastic strains $\{\Delta\varepsilon_j^{ne}\}$ for known increments ΔT and $\{\Delta\sigma_j\}$ using the microstructural model for SMA layer and bi-linear law for the elastoplastic layer. Denoting this operator by R, we write

$$\{\Delta\varepsilon_j^{ne}\} = R\big(\Delta T, \{\Delta\sigma_j\}\big).$$

Now we formulate the scheme of transition from the "vector" $\{\varepsilon_j^{ne}(t)\}$ corresponding to a time instant t to the

"vector" $\{\varepsilon_j^{ne}(t+\Delta t)\}$, where the time increment Δt corresponds to the increments ΔT, ΔM and ΔF of the temperature, the bending moment and the axial force. This scheme is as follows.

1. Choose the 0-th approximation $\{\varepsilon_j^{ne}\}^{(0)} = 0$ for "vector" $\{\varepsilon_j^{ne}\}$.
2. Find $\{\sigma_j\}^{(1)} = \mathrm{M}(M + \Delta M, F + \Delta F\{\varepsilon_j^{ne}\}^{(0)})$.
3. Find the 1-st approximation $\{\varepsilon_j^{ne}\}^{(1)} = \{\varepsilon_j^{ne}\}^{(0)} + \lambda \mathrm{R}(\Delta T, \{\Delta\sigma_j\}^{(1)})$.
4. Repeat steps 1 – 3 until $\max_j(\{|\varepsilon_j^{ne\,(i+1)} - \varepsilon_j^{ne\,(i)}|\}) < err$,

where λ is the iteration parameter ($0<\lambda\leq 1$) and err denotes the admissible error.

Thus, for given thermomechanical loading specified by the successive values of temperature T_k, bending moment M_k, and axial force F_k corresponding to time instants t_k, one can find the values $\{\varepsilon^{ne}(t_k)\}$ and $\{\sigma(t_k)\}$ as well as the values κ_k of the curvature (or the corresponding deflection w_k) and the relative elongation $\bar{\varepsilon}_k$.

4. Simulation results

For simulation the following parameters were chosen: length $l = 20$ mm, width $b = 10$ mm. The thickness of the SMA layer was $h_1 = 1.0$ mm. As for the elastoplastic layer, two values of thickness were taken: the thin one with $h_2 = 0.14$ and the thick one with $h_2 = 0.4$ mm. For the first value $h_2 = 0.14$ mm the elastoplastic layer and the SMA layer in the austenitic state have equal bending stiffness and for $h_2 = 0.4$ mm they have equal tensile stiffness.

For the SMA the characteristic temperatures M_f, M_s, A_s, A_f, were chosen 303, 323, 340 360 K, and the latent heat $q_0 = -135$ J/cm^3, the Young's modulus for austenite 80 GPa, for martensite 28 GPa. The Bain's deformation tensor was correspondent to the B2-B19' transformation in TiNi SMA. The elastoplastic material was characterized by the Young's modulus 200 GPa, yield limit 400 MPa and the hardening slope (plastic modulus) 2 GPa.

The simulated experiment consisted of the following stages.

1. Preliminary straining at temperature when the SMA is in martensite producing pseudo-plastic phase strain in the SMA layer and plastic strain in the bias layer.
2. Unloading.
3. Heating to provoke the shape recovery.
4. Cooling causing a repeated shape change.

Two ways of preliminary straining were considered:

(1) bending by applying a moment up to maximum effective strain $\kappa h/2 = 5\%$;
(2) stretching with fixed zero curvature (counter-moment is applied) up to maximum elongation 5%.

The preliminary deflection – moment diagram for bending of the beam with the thin elastoplastic layer

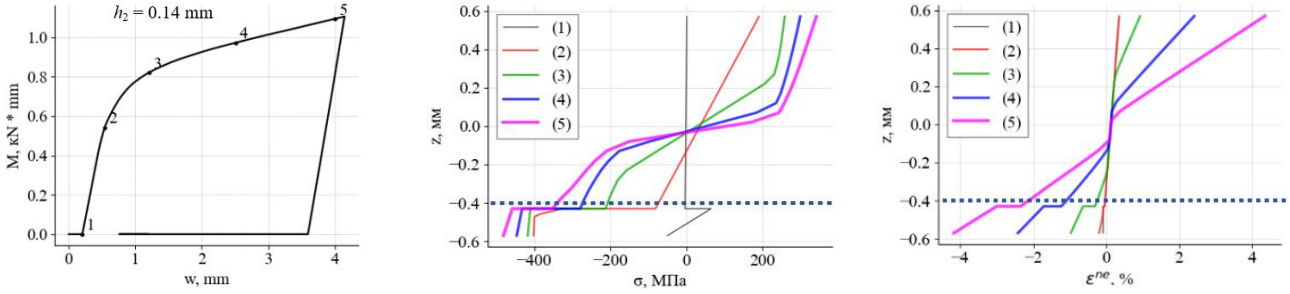

(a) Deflection – bending moment diagram

(b) Stress distributions over the thickness of the beam corresponding to marks 1 – 5 on the bending diagram

(c) Non-elastic strain distributions

Fig. 3 Bending of the beam with the thin elastoplastic layer ($h_2 = 0.14$ mm) at 300 K (SMA in the martensitic state)

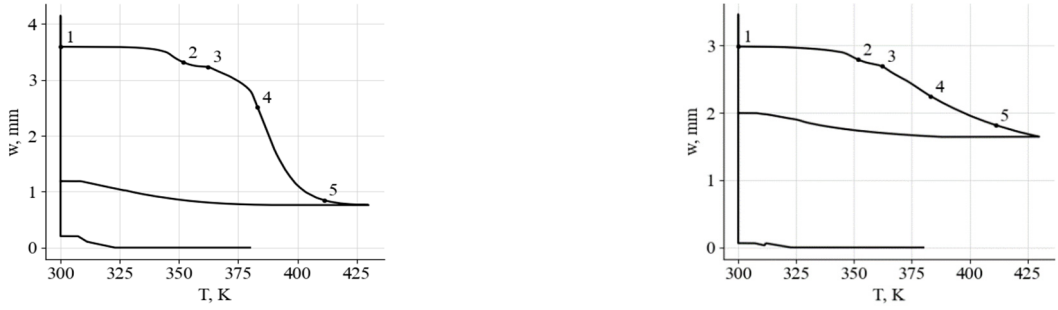

(a) $h_2 = 0.14$ mm

(b) $h_2 = 0.4$ mm

Fig. 4 Deflection vs. temperature diagrams on heating

$h_2 = 0.14$ mm is shown in Fig. 3(a) (the deflection correspondent to the center of the bent arc). From Fig. 3(b) one can see that the elastoplastic layer is completely under compressive stress. The upper part of the SMA layer is under tension and the lower part – under compression.

Note that the microstructural model automatically accounts for the tension-compression asymmetry of TiNi mechanical properties. The diagrams for the beam with thick elastoplastic layer 0.4 mm are similar to those shown in Fig. 3. On consequent heating after unloading the bent shape of the beam partially recovered. The temperature – deflection diagrams are presented in Fig. 4.

From Figs. 4(a), (b) one can see that the shape recovery is less for a beam with thick elastoplastic layer, since the SMA layer has to unbend this layer on heating. After heating the elastoplastic layer is under tensile stress, which can help regaining of the bent shape of the beam on subsequent cooling. From the stress distribution diagrams shown on Fig. 5 one can see that after the recovery the thin elastoplastic layer is completely under tensile load while the thick layer has the stress distribution characteristic to the elastoplastic bending, experiencing plastic deformation in its lower part. Thus, such thickness of the bias elastoplastic layer is too large and storing of the elastic energy is not efficient.

After shape recovery on heating cooling was simulated. The temperature dependence of the deflection can be seen on Fig. 4. In a larger scale it is presented in Fig. 6.

From Figs. 6 and 7 it follows that the deflection stroke on cooling is larger in the beam with thin bias layer. The stress distributions in the thin bias layer are linear, which is characteristic to the elastically bent beam. The stresses relax releasing the stored elastic energy. In the thick bias layer the relaxation of the stresses is not complete, which prevents regaining of the bent shape of the two-layer beam.

The second way of preliminary straining of the two-layer beam is its stretching at a temperature, at which the SMA is in the martensitic state, in constraint conditions, which prevent the beam bending. The force – elongation diagram for the beam with the thin bias layer is shown in Fig. 8. In both layers of the beam the stress distributions are uniform. After stretching the force is removed and that causes an increase of the moment (segment 5 – 6 on Fig. 8(b)). The moment is removed on the second stage of unloading (segment 6 – 7 on Fig. 8(b)). The diagrams for the beam with the thick bias layer are similar to those shown on Figs. 8 and 9.

Stress distributions over the thickness of the beam corresponding to marks 1 – 5 on the diagrams on Fig. 4 (the dashed lines show the position of the interface between the SMA and the elastoplastic layers).

After preliminary stretching up to 5% elongation and unloading the beam is slightly bent but the SMA layer is pre-stretched in the martensitic state and thus is capable to recover its initial length. Because of this on heating both of the layers acquire deflection. On subsequent cooling a part of this deflection is recovered. The dependences of the deflection on the temperature for the beam with the thin bias layer 0.14 mm are shown on Fig. 9(a) and the corresponding stress distributions – on Fig. 9(b).

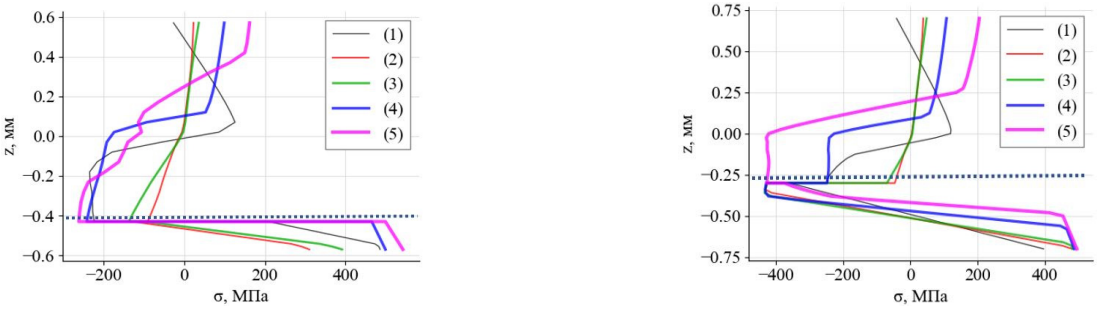

(a) $h_2 = 0.14$ mm (b) $h_2 = 0.4$ mm

Fig. 5 Stress distributions over the thickness of the beam corresponding to marks 1 – 5 on the diagrams on Fig. 4 (the dashed lines show the position of the interface between the SMA and the elastoplastic layers)

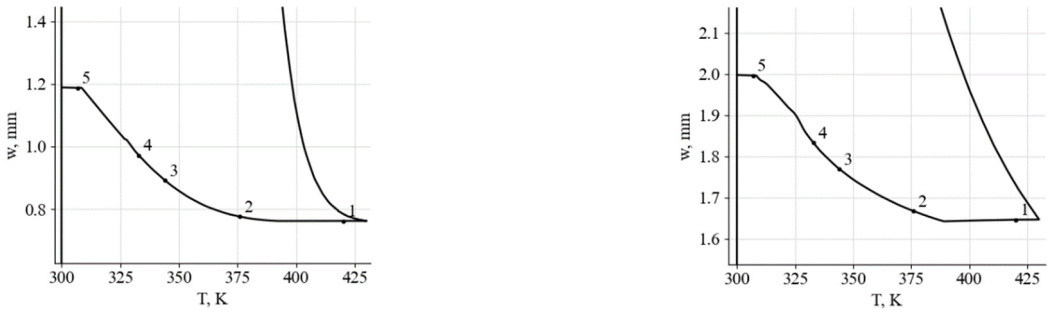

(a) $h_2 = 0.14$ mm (b) $h_2 = 0.4$ mm

Fig. 6 Deflection – temperature diagrams on cooling of the beam after the shape recovery

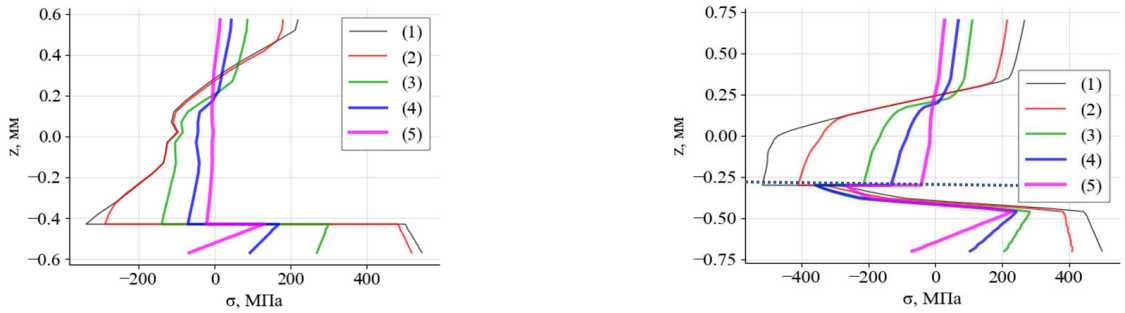

(a) $h_2 = 0.14$ mm (b) $h_2 = 0.4$ mm

Fig. 7 Stress distributions over the thickness of the beam corresponding to marks 1 – 5 on the diagrams on Fig. 6 (the dashed lines show the position of the interface between the SMA and the elastoplastic layers)

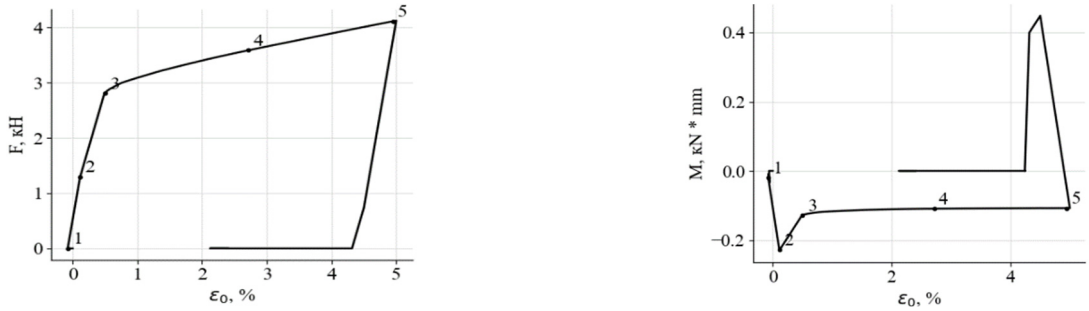

(a) Stretching force vs. relative elongation at 300 K (SMA in the martensitic state) (b) Moment vs. relative elongation

Fig. 8 Diagrams of stretching of a beam with thin bias layer ($h_2 = 0.14$ mm)

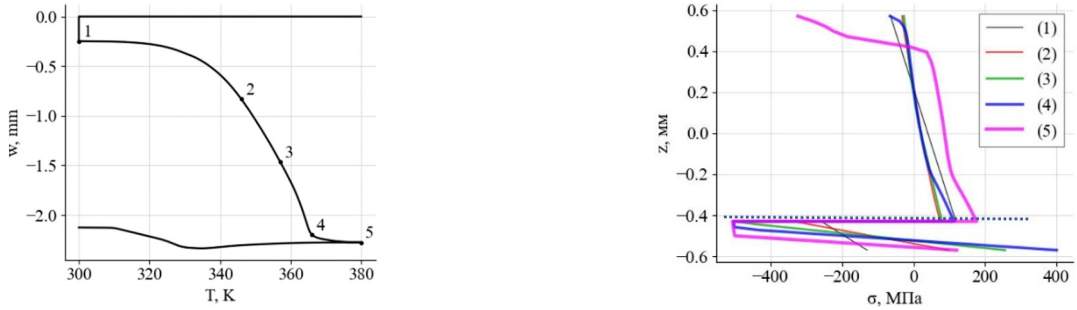

(a) Dependence of the beam deflection on the temperature (b) Stress distributions over the thickness of the beam corresponding to marks 1 – 5 on diagram on Fig. 9(a)

Fig. 9 Diagrams for heating and subsequent cooling of a beam with thin bias layer ($h_2 = 0.14$ mm)

5. Conclusions

1. Microstructural modeling allows solving boundary-value problems for thermomechanical loading of composite two-layer SMA – elastoplastic beam in the pure bending mode, revealing the inhomogeneity of the distributions of the stress.
2. Bimetal beams with functional and elastoplastic layers can recover the bent shape after preliminary straining both by bending or by stretching.
3. To obtain larger strain (deflection) variation on heating and on subsequent cooling the preliminary deformation must be performed by bending. The two-layer beam with thin elastoplastic layer is preferable: for preliminary bending up to maximum strain 5% the strain variation on heating will be 3.2% and on subsequent cooling 0.5%.

Acknowledgments

The research described in this paper was financially supported by the Russian Foundation of Basic Research 19-31-60035.

References

Ansys® Academic Research Mechanical APDL, Release 14.0, Help System, Material Reference/3.24, ANSYS, Inc.

Auricchio, F. and Petrini, L. (2002), "Improvements and algorithmical considerations on a recent three-dimensional model describing stress-induced solid phase transformations", *Int. J. Numer. Methods*, **55**(11), 1255-1284. https://doi.org/10.1002/nme.619

Belyaev, S., Rubanik, V., Resnina, N., Rubanik Jr, V., Rubanik, O. and Borisov, V.J.P.T. (2010a), "Martensitic transformation and physical properties of 'steel–TiNi' bimetal composite, produced by explosion welding", *Phase Transitions*, **83**(4), 276-283. https://doi.org/10.1080/01411591003656757

Belyaev, S., Rubanik, V., Resnina, N., Rubanik Jr, V., Rubanik, O., Borisov, V. and Lomakin, I. (2010b), "Functional properties of bimetal composite of "stainless steel – TiNi alloy" produced by explosion welding", *Physics Procedia*, **10**, 52-57. https://doi.org/10.1016/j.phpro.2010.11.074

Belyaev, S., Rubanik, V., Resnina, N. and Rubanik, O. (2011), "Effect of annealing on martensitic transformations in "steel – TiNi alloy" explosion welded bimetallic composite", *Metal Sci. Heat Treat.*, **52**(9), 432-436. https://doi.org/10.1007/s11041-010-9310-x

Belyaev, F.S., Evard, M.E. and Volkov, A.E. (2022), "Effect of plastic deformation on the martensitic transformations in TiNi alloy", *Smart Struct. Syst., Int. J.*, **29**(2), 311-319. https://doi.org/10.12989/sss.2022.29.2.311

Casciati, S. (2019), "SMA-based devices: insight across recent proposals toward civil engineering applications", *Smart Struct. Syst., Int. J.*, **24**(1), 111-125. https://doi.org/10.12989/sss.2019.24.1.111

Chatziathanasiou, D., Chemisky, Y., Meraghni, F., Chatzigeorgiou, G. and Patoor, E. (2015), "Phase transformation of anisotropic shape memory alloys: theory and validation in superelasticity", *Shape Memory Superelast.*, **1**, 359-374. https://doi.org/10.1007/s40830-015-0027-y

Duerig, T.W., Melton, K.N. and Stöckel, D. (eds.) (1990), *Engineering Aspects of Shape Memory Alloys*, Butterworth-Heinemann, New York, NY, USA.

Erglis, I.V., Ermolaev, V.A. and Volkov, A.E. (1995), "A model of martensitic unelasticity accounting for the crystal symmetry of the material", *Le Journal de Physique IV*, **5**(C8), 239-244. https://doi.org/10.1051/jp4:1995833

Evard, M.E. and Volkov, A.E. (1999), "Modeling of the martensite accommodation effect on mechanical behavior of shape memory alloys", *J. Eng. Mater. Technol.*, **121**, 102-104.

Evard, M.E., Volkov, A.E. and Bobeleva, O.V. (2006), "An approach for modelling fracture of shape memory alloy parts", *Smart Struct. Syst., Int. J.*, **2**(4), 357-363. https://doi.org/10.12989/sss.2006.2.4.357

Evard, M.E., Volkov, A.E. and Belyaev, F.S. (2015), "A microstructural model of SMA with microplastic deformation and defects accumulation: Application to thermocyclic loading", *Materials Today: Proceedings*, **2**(3), S583-S587. https://doi.org/10.1016/j.matpr.2015.07.352

Fall, M.D., Patoor, E., Hubert, O. and Lavernhe-Taillard, K. (2019), "Comparative study of two multiscale thermos-mechanical models of polycrystalline shape memory alloys: Application to a representative volume element of titanium–niobium", *Shape Memory Superelast.*, **5**, 163-171. https://doi.org/10.1007/s40830-019-00216-7

Fischlschweiger, M., Oberaigner, E.R., Antretter, T. and Cailletaud, G. (2011), "A multi-block-spin approach for martensitic phase transformation based on statistical physics", *Proceedings of Behavior and Mechanics of Multifunctional Materials and Composites*, Vol. 7978, pp. 398-405, San Diego, CA, USA. https://doi.org/10.1117/12.881960

Huang, M. and Brinson, L.C. (1998), "A multivariant model for single crystal shape memory alloy behavior", *J. Mech. Phys. Solids*, **46**(8), 1379-1409. https://doi.org/10.1016/S0022-5096(97)00080-X

Imamura, T., Nishiura, T., Kawano, H., Hosoda, H. and Nishida, M. (2012), "Self-accommodation of B19' martensite in Ti-Ni shape memory alloys – Part III. Analysis of habit plane variant clusters by the geometrically nonlinear theory", *Philosophical Magazine*, **92**, 2247-2263.

Jani, J.M., Leary, M., Subic, A. and Gibson, M.A. (2014), "A review of shape memory alloy research, applications and opportunities", *Mater. Des.*, **56**, 1078-1113. https://doi.org/10.1016/j.matdes.2013.11.084

Kukhareva, A., Kozminskaia, O. and Volkov, A. (2020), "Calculation of the transformation plasticity strain in the shape memory cylinder", In: *E3S Web of Conferences*, Vol. 157, p. 06016. https://doi.org/10.1051/e3sconf/202015706016

Lagoudas, D.C. (2008), *Shape Memory Alloys: Modeling and Engineering Applications*, Springer, Berlin, Germany.

Li, Q., Seelecke, S., Kohl, M. and Krevet, B. (2006), "Thermo-mechanical finite element analysis of a shape memory alloy cantilever beam", *Proceedings of SPIE 6166, Smart Structures and Materials 2006: Modeling, Signal Processing, and Control*, Vol. 6166, pp. 562-569.San Diego, CA, USA, March, SPIE 06-6166-73. https://doi.org/10.1117/12.677238

Likhachev, V.A., Razov, A.I. and Volkov, A.E. (1997), "Finite difference simulation of a thermomechanical coupling", A.R. Pelton, D. Hodgson, S.M. Russel, T. Duerig (eds.), *Proceedings of the Second International Conference on Shape Memory and Superelastic Technologies SMST-97*, March, Pacific Grove, CA, USA, pp. 335-340.

Nae, F.A., Matsuzaki, Y. and Ikeda, T. (2003), "Micromechanical modeling of polycrystalline shape-memory alloys including thermo-mechanical coupling", *Smart Mater. Struct.*, **12**, 6-17. https://doi.org/10.1088/0964-1726/12/1/302

Niclaeys, C., Zineb, T.B. and Patoor, E. (2004), "Influence of microstructural parameters on shape memory alloys behavior", Ahzi, S., Cherkaoui, M., Khaleel, M.A., Zbib, H.M., Zikry, M.A. and Lamatina, B. (eds.), *Proceedings of IUTAM Symposium on Multiscale Modeling and Characterization of Elastic-Inelastic Behavior of Engineering Materials. Solid Mechanics and Its Applications*, Vol. 114, Springer, Dordrecht, The Netherlands. https://doi.org/10.1007/978-94-017-0483-0_33

Nishida, M., Nishiura, T., Kawano, H. and Imamura, T. (2012a), "Self-accommodation of B19′ martensite in Ti-Ni shape memory alloys – Part I. Morphological and crystallographic studies of variant selection rule", *Philosophical Magazine*, **92**, 2215-2233.

Nishida, M., Okunishi, E., Nishiura, T., Kawano, H., Imamura, T., Ii, S. and Hara, T. (2012b), "Self-accommodation of B19' martensite in Ti-Ni shape memory alloys – Part II. Characteristic interface structures between habit plane variants", *Philosophical Magazine*, **92**, 2234-2246.

Oberaigner, E.R. and Leindl, M. (2012), "Statistical physics concepts for the explanation of effects observed in martensitic phase transformations", *Smart Mater. Struct.*, **21**(9), 094020. https://doi.org/10.1088/0964-1726/21/9/094020

Patoor, E, Eberhardt, A. and Berveiller, M. (1996), "Micromechanical modelling of superelasticity in shape memory alloys", *J. de Physique IV*, **6**(C1), 277-292. https://doi.org/10.1051/jp4:1996127

Petrini, L., Bertini, A., Berti, F., Pennati, G. and Migliavacca, F. (2017), "The role of inelastic deformations in the mechanical response of endovascular shape memory alloy devices", *J. Eng. Med.*, **231**(5), 391-404. https://doi.org/10.1177/0954411917696336

Prummer, R. and Stockel, D. (2001), "NITINOL - stainless steel compound material, made by explosion welding", K.P. Staudhammer, L.E. Murr, and M.A. Meyers (eds.), In: *Fundamental Issues and Applications of Shock-Wave and High-Strain-Rate Phenomena*, Elsevier, pp. 581-584.

Rogovoy, A.A. and Stolbova, O.S. (2019), "Numerical simulation of the phase transition control in torsion of a hollow cylinder made of Heusler alloy", *PNRPU Mech. Bull.*, (3), 75-87.

Salzbrenner, R.J. and Cohen, M. (1979), "On the thermodynamics of thermoelastic martensitic transformations", *Acta Metallurgica*, **27**(5), 739-748. https://doi.org/10.1016/0001-6160(79)90107-X

Simoes, M. and Martínez-Pañeda, E. (2021), "Phase field modelling of fracture and fatigue in Shape Memory Alloys", *Comput. Methods Appl. Mech. Eng.*., **373**, 113504. https://doi.org/10.1016/j.cma.2020.113504

Torra, V., Carreras, G., Casciati, S. and Terriault, P. (2014), "On the NiTi wires in dampers for stayed cables", *Smart Struct. Syst.*, *Int. J.*, **13**(3), 353-374. https://doi.org/10.12989/sss.2014.13.3.353

Volkov, A.E. and Casciati, F. (2001), "Simulation of dislocation and transformation plasticity in shape memory alloy polycrystals", Auricchio F, Faravelli L, Magonette G and Torra V (eds.), In: *Shape Memory Alloys. Advances in Modelling and Applications*, Barcelona, Spain, pp. 88-104.

Volkov, A.E. and Kukhareva, A.S. (2008), "Calculation of the stress-strain state of a TiNi cylinder subjected to cooling under axial force and unloading", *Bull. Russian Acad. Sci.: Phys.*, **72**(9), 1267-1270. https://doi.org/10.3103/S106287380809027X

Volkov, A.E., Emelyanova, E.V., Evard, M.E. and Volkova, N.A. (2013), "An explanation of phase deformation tension–compression asymmetry of TiNi by means of microstructural modeling", *J. Alloys Compounds*, **577**(S1), S127-S130. https://doi.org/10.1016/j.jallcom.2012.05.131

Volkov, A.E., Kukhareva, A.S., Volkova, N.A. and Malkova, Y.V. (2017), "Size effects in a shape memory alloy rod caused by inhomogeneity of temperature and stress fields studied through solving of a 1d connected thermal and mechanical problem", *Proceedings of the 8th Conference on Smart Structures and Materials*, *SMART 2017 and 6th International Conference on Smart Materials and Nanotechnology in Engineering*, January, pp. 1582-1589.

Volkov A.E., Evard, M.E., Volkova, N.A. and Vukolov, E.A. (2019), "Application of a microstructural model to simulation of a TiNi beam bending performance and calculation of thickness stress distributions", *Proceedings of the 9th ECCOMAS Thematic Conference on Smart Structures and Materials*, *SMART 2019*, pp. 686-695.

Wanhill, R.J.H. and Ashok, B. (2017), "Shape Memory Alloys (SMAs) for Aerospace Applications", Prasad, N., Wanhill, R. (eds.), In: *Aerospace Materials and Material Technologies*, Indian Institute of Metals Series, Springer, Singapore.

Yang, S. and Seelecke, S. (2008), "Modeling and analysis of SMA-based adaptive structures", *Proceedings of the COMSOL Conference 2008*, Boston, MA, USA.

Zhang, W., Zhang, Y., Zheng, G., Zhang, R. and Wang, Y. (2013), "A biomechanical research of growth control of spine by shape memory alloy staples", *BioMed Res. Int.*, 384894. https://doi.org/10.1155/2013/384894